Band alignment and electronic structure of the anatase $TiO_2/SrTiO_3(001)$ heterostructure integrated on Si(001)

Hosung Seo,[1] Agham B. Posadas,[1] Chandrima Mitra,[1] Alexander V. Kvit,[2] Jamal Ramdani,[3] and Alexander A. Demkov[1,*]

[1]*Department of Physics, The University of Texas at Austin, Austin, Texas 78712, USA*

[2]*Department of Materials Science and Engineering, University of Wisconsin—Madison, Madison, Wisconsin 53706, USA*

[3]*National Semiconductor, Santa Clara, California 95052, USA*

(Received 21 May 2012; published 1 August 2012)

Using density functional theory (DFT), scanning transmission electron microscopy (STEM), and electron energy loss spectroscopy (EELS), we study the interface structure and electronic properties of the anatase-$TiO_2/SrTiO_3(001)$ heterostructure epitaxially grown on Si(001) by molecular beam epitaxy (MBE). We show that charge transfer at the $TiO_2/SrTiO_3$ interface is induced by the chemical bond formation between Ti and O. Subsequent O lattice polarization is found to be the leading screening mechanism at the interface. By comparing the theoretical local electronic structure to the O *K* edge EELS spectra taken at the interface with atomic resolution, we are able to trace how the local band structure evolves in response to the change in symmetry and bonding across the interface. We also discuss the effect of interfacial point defects (O vacancy and F impurity) on the band alignment.

DOI: 10.1103/PhysRevB.86.075301 PACS number(s): 73.20.−r, 81.15.−z

I. INTRODUCTION

Anatase TiO_2 is the subject of extensive research effort due to its energy and environmental applications.[1–4] The conduction band edge of TiO_2 is well matched to the redox potential of water, making it an excellent candidate for hydrogen production via photocatalytic water splitting.[5] This material system is promising due to its relatively high efficiency, chemical stability in water, nontoxicity, and low production cost.[1] Among the three polymorphs of TiO_2 (rutile, anatase, and brookite), the most abundant phase in nature is rutile (space group $P4_2/mnm$). However, it has been found that anatase (space group $I4_1/amd$) shows significantly higher photocatalytic activity than rutile.[5] This has been attributed to the higher reactivity of the anatase (001) surface,[6,7] higher mobility of the charge carriers,[8,9] and longer electron-hole pair lifetime.[10]

The main challenge for photocatalytic applications is the rather large band gap of anatase TiO_2 (approximately 3.2 eV, making it ultraviolet active) and high recombination rate of the photoexcited electron-hole pairs.[11] A variety of methods for band-gap engineering have been proposed to utilize solar-abundant visible light instead of ultraviolet, including nitrogen doping,[12] codoping,[13,14] and surface hydrogenation.[15] In order to overcome these challenges, oxide interface engineering has attracted considerable attention.[16–19] In addition to band-gap engineering at the interface, a longer lifetime of photoexcited electron-hole pairs could be achieved, for example, by spatially separating the carriers across the interface using a staggered band alignment. However, a clear understanding of the interface effects on the photocatalytic activity of mixed oxide catalysts is lacking, in particular due to a limited number of model systems where such a connection can be traced.[20]

Since the thermodynamically stable bulk phase of TiO_2 at room temperature and ambient pressure is rutile, single-crystal anatase is typically synthesized only in the form of nanoparticles.[2,6] However, recent advances in oxide heteroepitaxy have made it possible to grow high-quality, single-crystal anatase films on perovskite substrates such as $SrTiO_3$ (STO) or $LaAlO_3$ (LAO).[21,22] This provides an excellent model system for controlled studies of the photocatalytic behavior of anatase under various conditions.[23–25] Burbure *et al*. have shown that for anatase-$TiO_2/BaTiO_3$ structures, dipole fields from the underlying ferroelectric domains separate holes and electrons, leading to spatially selective photochemical reactions at the anatase surface.[23] Kazazis and coworkers have reported that the photocatalytic activity at the surface of anatase deposited on Si(111) can be controlled by changing the Fermi level position of the Si substrate.[24] Moreover, a number of interesting physical phenomena and potential applications of anatase/perovskite oxide heterostructures have been reported, including thermoelectric and spintronic applications.[26–30]

While a considerable amount of experimental work can be found in the literature, a detailed theoretical understanding of the electronic structure of the anatase-TiO_2/perovskite interface is lacking. Such knowledge could suggest new ways of manipulating the band structure and band alignment, which are crucial in high-efficiency hydrogen production using sunlight, making this system of significant fundamental and practical interest. Recently, Chambers *et al*., using x-ray photoelectron spectroscopy (XPS), have reported that there is no measurable valence band offset between anatase $TiO_2(001)$ and STO(001).[31] Curiously, in contradiction with the XPS result, their density functional theory (DFT) calculations suggest a valence band offset of 0.5 eV. This could be interpreted either as the inability of DFT to fully account for the interface properties or that the atomic structure used in the calculation differs from the experimental one. We feel that, in view of its importance, the band alignment problem at this interface warrants revisiting.

In this paper, we consider a heterojunction of anatase with STO grown on Si. Using molecular beam epitaxy (MBE), we grew epitaxial *c*-axis-oriented anatase on an STO/Si(001) pseudosubstrate,[32] and used *Z*-contrast scanning transmission electron microscopy (STEM) to elucidate the real physical structure of the interface. Electron energy loss spectroscopy (EELS) was used to probe the electronic structure across

the interface. The interface geometry inferred from STEM was used in DFT calculations, which were then validated by comparing the theoretical density of states with the O K edge EELS structure.

The paper is organized as follows: First, we briefly introduce the computational methodology used in the paper and describe the anatase MBE growth. This is then followed by a detailed analysis of the electronic structure of the interface, including charge transfer, dielectric screening, and the possible role of point defects.

II. METHODOLOGY

A. Theory

We used DFT as implemented in the VASP code.[33] The exchange-correlation energy is treated within the local density approximation (LDA), using the Ceperley-Alder data parameterized by Perdew and Zunger.[34] We employed projector-augmented wave pseudopotentials to describe Sr, Ti, and O.[35] Valence electron configurations for the elements were $4s^2 4p^6 5s^2$ for Sr, $3d^2 4s^2$ for Ti and $2s^2 2p^4$ for O. We used a cutoff energy of 600 eV for the plane-wave expansion. The electronic total energy was converged to 10^{-6} eV/cell. We fully relaxed the internal ionic degrees of freedom until the Hellmann-Feynman forces were less than 10 meV/Å. We employed $6\times6\times6$ and $6\times6\times4$ Monkhorst-type k-point meshes to integrate over the Brillouin zone for cubic STO and tetragonal anatase TiO_2, respectively. We calculated the STO lattice parameter a to be 3.873 Å and the TiO_2 lattice parameters a and c to be 3.766 Å and 9.456 Å ($c/a = 2.511$), respectively. These are in good agreement with low temperature experimental values of $a = 3.897$ Å for STO[36] and $a = 3.780$ Å and $c = 9.491$ Å ($c/a = 2.511$) for anatase TiO_2[37] that are extrapolated based on the thermal expansion coefficients. Thus, theoretical biaxial tensile strain in the anatase film on STO(001) was calculated to be 2.8%, which agrees well with the experimental value of 3.0%.

To model the evolution of the valence band with the anatase film thickness, we used several supercells. We modeled the substrate with a five-unit-cell-thick TiO_2-terminated STO(001) slab. We considered four, six, and eight monolayers (MLs) of anatase (one anatase unit cell has four MLs) on both sides of STO to take into account any interface and surface dipoles within the periodic boundary conditions. The supercell with eight MLs of anatase is shown in Fig. 1. The slab in each computational cell was separated from its nearest-neighbor images in the c direction by 14 Å of vacuum to avoid spurious slab-slab interactions. We considered two types of supercells in terms of the in-plane cell size. To study the basic properties of the interface, we used a 1×1 in-plane

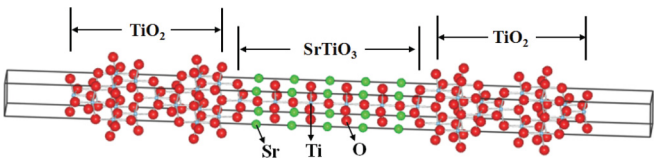

FIG. 1. (Color online) Slab model of the eight-ML anatase $TiO_2/SrTiO_3(001)$ heterostructure.

cell. We increased the cell size to $\sqrt{2}\times\sqrt{2}$ to calculate the O K-edge spectra, O vacancy, and F impurity at the interface. We used a $6\times6\times2$ k-point mesh for the 1×1 supercells. For the $\sqrt{2}\times\sqrt{2}$ calculations, a $4\times4\times2$ k-point grid was used for the structural relaxation while a $6\times6\times2$ grid was used for the total energy and density of states calculations.

To investigate whether the LDA causes the incorrect band offset prediction as suggested in Ref. 31, we used a quasiparticle (QP) correction within the G_oW_o approximation as implemented in the VASP code.[38] In principle, the QP energies were obtained by solving the equation

$$(T + V_{\text{ext}} + V_H)\psi_{nk}(\mathbf{r}) + \int \mathbf{dr}'\Sigma(\mathbf{r},\mathbf{r}' : E_{nk})\psi_{nk}(\mathbf{r}') = E_{nk}\psi_{nk}(\mathbf{r}), \quad (1)$$

where T is the kinetic energy of the electrons, V_{ext} is the external potential of the ions, and V_H is the Hartree potential. The energy-dependent nonlocal self-energy operator Σ contains the exchange and correlation effects, and, within Hedin's GW approximation,[39], it takes the form

$$\Sigma(\mathbf{r},\mathbf{r}' : \omega) = \frac{i}{4\pi}\int_{-\infty}^{\infty} e^{i\omega'\delta}G(\mathbf{r},\mathbf{r}',\omega+\omega')W(\mathbf{r},\mathbf{r}',\omega')d\omega', \quad (2)$$

where G is the Green's function and W is the screened Coulomb interaction. Then, to first order, the QP eigenvalues of equation (1) are obtained as

$$E_{nk}^{\text{QP}} = \langle\psi_{nk}|T + V_{\text{ext}} + V_H + \Sigma|\psi_{nk}\rangle. \quad (3)$$

In a non-self-consistent G_0W_0 approximation, which has been shown to be a quite reasonable approximation,[39,40] the ψ_{nk} were chosen to be the Kohn-Sham LDA wave functions. For our calculations we chose a plane-wave cutoff of 680 eV for both STO and TiO_2. The number of bands used is 300 and 620 for STO and TiO_2, respectively. For the frequency integration in Eq. (2), we used 50 frequency grid points. The QP eigenvalues were converged to 0.03 eV.

B. Experiment

Anatase was deposited using MBE on a $SrTiO_3$ layer that was epitaxially grown on Si(001). The Si wafer was first degreased and then exposed to ultraviolet/ozone prior to loading into the growth chamber. After desorption of the native SiO_2 using a Sr-assisted deoxidation process,[41] 50 Å of crystalline $SrTiO_3$ with TiO_2 termination was deposited on Si with the aid of a 1/2 monolayer Sr template[32,42] at a substrate temperature of 550 °C and a background oxygen pressure of 4×10^{-7} torr. The substrate temperature was then quickly increased to 650 °C, while oxygen pressure was slowly ramped to 1×10^{-6} torr for the anatase TiO_2 deposition. Samples with total thicknesses of 10–40 monolayers of anatase (one anatase unit cell equals 4 MLs) were deposited on $SrTiO_3$/Si. The growth of all the layers was monitored *in situ* using reflection high-energy electron diffraction (RHEED). Typical RHEED patterns for both $SrTiO_3$ and anatase are shown in Fig. 2. Figure 2(a) shows a RHEED pattern taken along the Si⟨110⟩ ($SrTiO_3$⟨100⟩) direction for a 5-nm $SrTiO_3$ film grown on Si(001). Figure 2(b) shows a RHEED

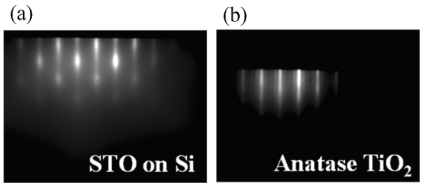

FIG. 2. RHEED patterns for (a) an STO film on Si(001) taken along the Si⟨110⟩ direction; and (b) for a 20-ML anatase film taken along the same direction (b).

pattern for a 20-ML anatase film taken along the same direction. The anatase surface shows a 4×1 surface reconstruction typically exhibited by well-ordered epitaxial anatase films.[21]

After growth, the samples are prepared for cross-section transmission electron microscopy by polishing and dimpling. Samples are thinned to electron transparency using a low-angle stage for the Fischione 1010 ion mill. STEM measurements were performed on a FEI Titan 80-300 electron microscope operated at 200 kV and configured with a CEOS probe-side aberration corrector, which allowed us to achieve a resolution 0.78 Å at working parameters. Figure 3 shows a high-resolution Z-contrast image of the interface. This image is taken along the Si[110] zone axis. It shows a well-ordered epitaxial relationship among the Si substrate, STO, and TiO_2. The most likely interface structure is shown by the overlay in Fig. 3. This interface structure is used as the starting model in the DFT calculations.

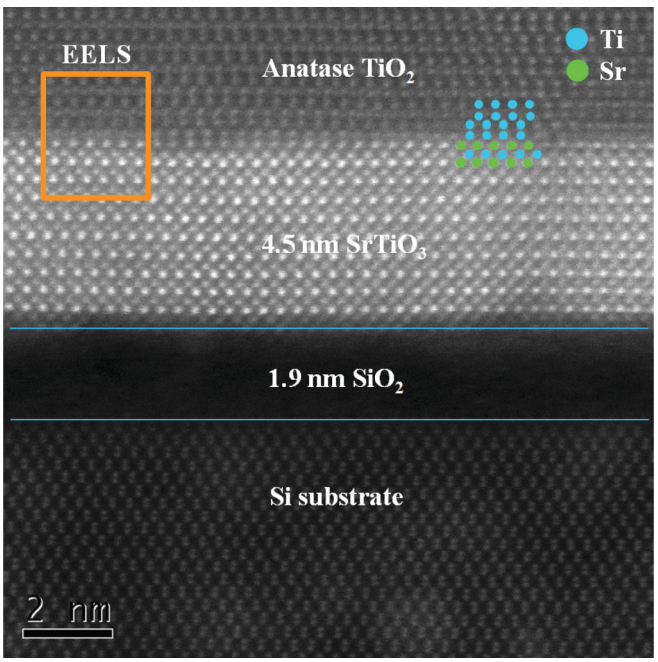

FIG. 3. (Color online) Z-contrast HRTEM image of the $TiO_2/SrTiO_3/Si(001)$ structure. Blue (Ti) and green (Sr) balls are superimposed at the $TiO_2/SrTiO_3$ interface as a guide to the eye. Spatially resolved EELS measurement is performed at the region indicated by the orange box.

III. RESULTS AND DISCUSSION

The band offset is the fundamental physical parameter that largely affects the functionality of a heterostructure, due to its profound effect on the carrier confinement and electronic transport along and across the interface. However, oxide heterointerfaces are not as well understood as those between metals and semiconductors. The band alignment at oxide heterointerfaces has attracted considerable attention in the context of the high-k dielectric gate stack in field-effect transistors.[43–47] More recently, the band alignment between complex oxides has been of great interest following the discovery of novel interfacial electronic phases emerging at the epitaxial complex oxide heterointerfaces.[48–51] To describe and control the band alignment between two materials, the interfacial chemistry of a given heterointerface has to be well understood.[44,45,52–54]

A. Charge transfer and dielectric screening at the interface

To understand the mechanism of the band offset formation at the anatase/STO interface, let us first consider the Schottky limit when two oxide slabs are far apart so there is no interaction between them. We consider TiO_2-terminated STO(001) and tensile-strained (2.8%) anatase TiO_2(001) slabs separately. The calculated planar-averaged electrostatic potential of these isolated slabs as a function of distance in the (001) direction is shown in Fig. 4. By macroscopically averaging the potentials, we identify the reference energy positions[55–57] in the bulk regions of STO(001) and TiO_2 with respect to the vacuum level, which is set at 0 eV. The relative position of the valence band maximum (VBM) with respect to the reference energy is then determined in two separate bulk calculations. Assuming a common vacuum level, we find the valence band offset ΔE_v $[= E_{\mathrm{VBM}}(\mathrm{STO}) - E_{\mathrm{VBM}}(\mathrm{TiO_2})]$ to be 0.94 eV. The offset changes to 0.89 eV if a relaxed anatase film ($a = b =$ 3.766 Å) is considered, meaning that in the Schottky limit, tensile strain plays only a minor role in determining the band offset. The relatively large valence band offset can be traced to the difference in oxygen coordination between the two oxides, since in both materials the top of the valence band is formed predominantly by the oxygen p states. This point will be further discussed in Sec. III B.

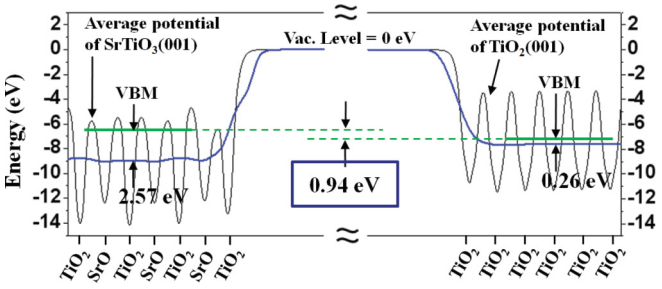

FIG. 4. (Color online) Planar-averaged electrostatic potentials along the (001) direction for free-standing STO (left) and TiO_2 slabs (right). Macroscopically averaged potential profiles are shown in blue. Energy position of valence band maximum (VBM) in the bulk region of each slab with respect to the reference potential energy is indicated with the green line. Dotted green lines are drawn for comparison of the two VBM positions to visualize the Schottky-limit band offset.

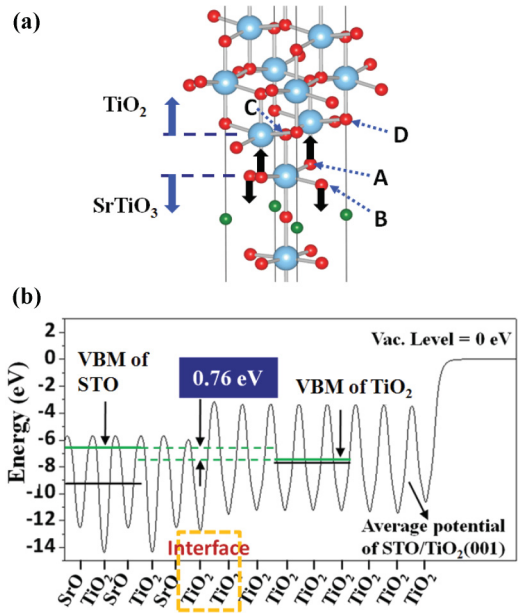

FIG. 5. (Color online) (a) Interface model between anatase TiO_2 and STO(001). Black arrows show the relaxation pattern of the O ions at the interface. (b) Planar-averaged electrostatic potential of the heterostructure along the (001) direction. The straight black lines indicate the reference electrostatic energy positions with respect to the vacuum level (0 eV) in the bulk region of STO and TiO_2, respectively. The green lines indicate the relative positions of VBM of STO and TiO_2 with respect to their corresponding reference energy positions.

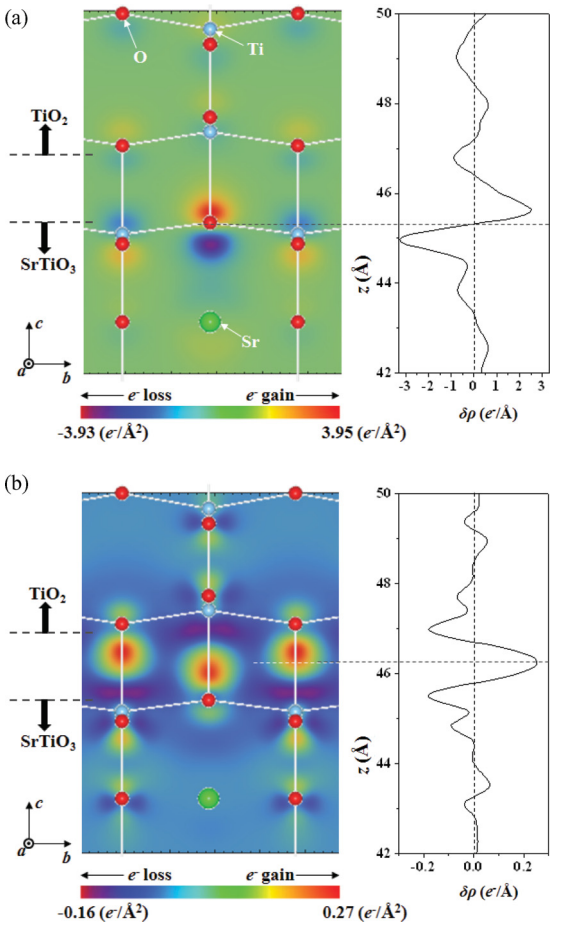

FIG. 6. (Color online) Two-dimensional (left) and one-dimensional (right) projections of the charge redistribution $[\delta\rho(x,y,z)]$ at the $TiO_2/SrTiO_3(001)$ interface (see text). For the reference charge density of the free-standing STO and TiO_2 slabs, we use relaxed (a) or unrelaxed (b) atomic geometry.

When two oxide slabs are brought into contact, chemical bonds are created that result in charge redistribution in conjunction with a structural distortion at the interface. Our physical interface model between anatase TiO_2 and STO(001) is shown in Fig. 5(a) and is based on the STEM image in Fig. 3. Note that half of O at the "STO surface" is bonded to Ti of anatase, leading to threefold-coordinated O ($O_{3\text{-fold}}$, site A), while the other half of O remains twofold coordinated ($O_{2\text{-fold}}$, site B). Ti at the STO surface is also bonded to O of anatase at site C. We first check the evolution of the interface electronic structure as four-, six-, or eight-ML TiO_2 films are "deposited" (one anatase unit cell has four TiO_2 MLs). There is no significant change in the interface electronic structure for the different coverages, and, furthermore, after deposition of six MLs, the bulk electronic structure is recovered in the middle layer of the anatase region. In what follows, we focus on the heterostructure with eight MLs of anatase deposited on STO(001) (see Fig. 1) unless otherwise noted.

The valence band offset of the heterostructure can be written as $\Delta E_H = \Delta E_S + \Delta V$, where ΔE_H is the band offset of the actual heterostructure, ΔE_S is the band offset in the Schottky limit, and ΔV is the electrostatic potential drop at the interface due to the heterojunction formation. The valence band offset is calculated using the macroscopic average of the electrostatic potential,[55–57] as shown in Fig. 5(b). We calculate the valence band offset to be 0.76 eV, thus ΔV is -0.2 eV. This process is often described as the creation of an interface dipole or double layer involving charge transfer and subsequent dielectric screening at the interface.[44,45]

Based on the Schottky limit result, we expect electron transfer from the STO valence band into TiO_2. There are two channels for charge transfer: chemical bond induced transfer[58] and transfer into evanescent gap states.[59] In Fig. 6, we show the charge redistribution at the interface, which is defined as

$$\delta\rho(x,y,z) = \rho(\text{heterostructure}) - \rho(\text{STO substrate}) - \rho(\text{TiO}_2\text{ film}), \quad (4)$$

where ρ is the valence charge density of a given structure. In Fig. 6(a), we use the charge densities of the relaxed free-standing STO and TiO_2 slabs for ρ(STO substrate) and ρ(TiO_2 film), respectively, while for the plots in Fig. 6(b) we use those of the STO and TiO_2 slabs where ionic positions are kept as those in the heterostructure. The two-dimensional (2D) and one-dimensional (1D) projections are defined as

$$\delta\rho(y,z) = \int_0^a \delta\rho(x,y,z)dx \quad \text{and}$$
$$\delta\rho(z) = \int_0^a \int_0^a \delta\rho(x,y,z)dxdy, \quad (5)$$

respectively, where a is the STO lattice parameter. First, we note that the charge transfer is better represented in Fig. 6(a)

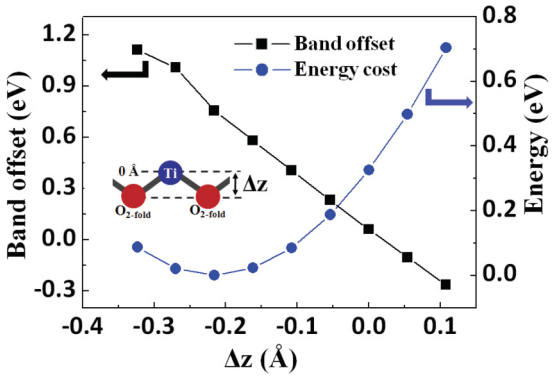

FIG. 7. (Color online) Band offset and total energy of the TiO_2/STO heterostructure as a function of the displacement of $O_{2\text{-fold}}$ ions at the interface. The inset is a schematic picture to show the lattice polarization by $O_{2\text{-fold}}$ at the interface. In the relaxed heterostructure, the optimal Δz is -0.22 Å, where the energy is minimum.

than in Fig. 6(b). We then observe that, indeed, chemical bonds drive the charge transfer between O and Ti. Assuming that the chemical bonds locally modify the charge density, the density underneath the STO surface is shifted upward (toward anatase) and localized along the chemical bonds between O and Ti, as shown in Fig. 6(a). The charge transfer to evanescent states of TiO_2 decays rapidly within two MLs of anatase, as seen in Fig. 8(a), where the finite density of states in the gap (between zero and -1 eV) can be seen only in the first two MLs of anatase.

For oxide interfaces, Sharia *et al.* have pointed out the importance of screening by use of O lattice polarization.[44] They have shown that as the coordination number of interfacial O increases, the Born effective charge of O increases as well and, as a result, the band offset is pushed back to the Schottky limit due to the enhanced screening ability of interfacial O. The same argument applies to the $TiO_2/SrTiO_3$ structure. We note that the $O_{2\text{-fold}}$ ions at the interface shift by 0.22 Å from the Ti plane toward the STO bulk side as shown in Fig. 5(a). In Fig. 7, we show the calculated band offset as a function of position of the $O_{2\text{-fold}}$ ions in the (001) direction. Pushing the $O_{2\text{-fold}}$ ions back to the level of the Ti plane decreases the band offset from 0.76 to 0.06 eV. It suggests that lattice polarization by the $O_{2\text{-fold}}$ ions is indeed the main screening mechanism at the interface.[44] The potential change at the interface due to lattice polarization is given by[60,61]

$$\Delta V(O_{2\text{-fold}}) = \frac{1}{a^2}\frac{Z^{*(T)}_{O_{2\text{-fold}}}}{\varepsilon_0\varepsilon_\infty}\Delta u(O_{2\text{-fold}}), \qquad (6)$$

where a is the in-plane lattice parameter, $Z^{*(T)}_{O_{2\text{-fold}}}$ is the Born effective charge of $O_{2\text{-fold}}$ along the (001) direction, $\Delta u(O_{2\text{-fold}})$ is the displacement of $O_{2\text{-fold}}$ with respect to the Ti plane in the (001) direction and ε_∞ is the optical dielectric constant. Assuming $\varepsilon_\infty \approx 6.2$,[62–64] we estimate the Z^* of $O_{2\text{-fold}}$ at the interface to be -1.66. This number is consistent with the model developed in Ref. 44.

To gain further insight, we analyze the spatial evolution of the electronic structure of the anatase layer from the interface with STO to the surface. We plot the layer-by-layer projected density of states (pDOS) for the valence band in Fig. 8(a).

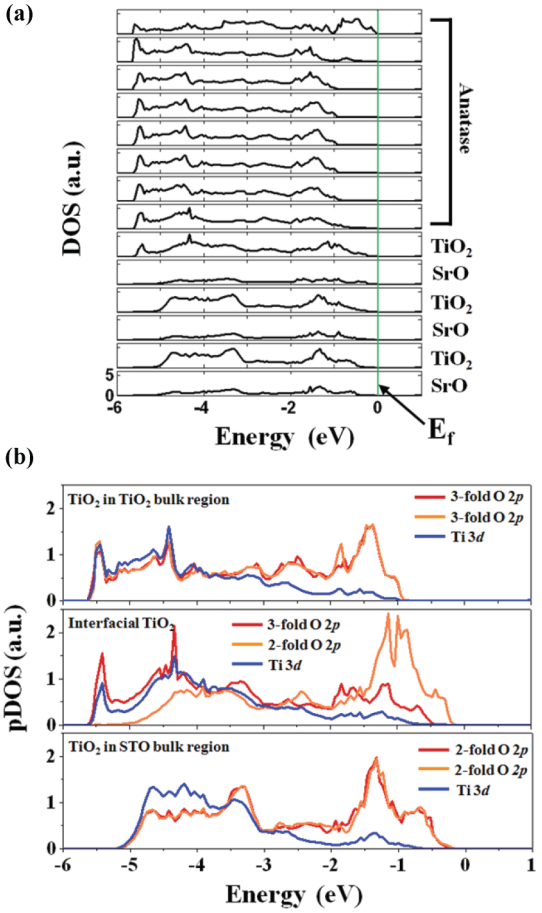

FIG. 8. (Color online) (a) Layer-by-layer projected density of states (pDOS) of the $TiO_2/SrTiO_3$(001) heterostructure. The green line is the Fermi level. (b) Atom-resolved pDOS of the TiO_2 layer at the STO bulk (bottom), interface (middle), and TiO_2 bulk (top) regions.

Noting that the middle layers of the TiO_2 film recover the bulk electronic structure, we find a valence band offset of 0.7 eV, consistent with that obtained by the average potential method. We plot the pDOS corresponding to Ti d orbitals and O p orbitals of a TiO_2 layer in the STO bulk region, the interfacial TiO_2 layer, and a TiO_2 layer in the bulk region of anatase in Fig. 8(b). By comparing the pDOS of $O_{2\text{-fold}}$ and $O_{3\text{-fold}}$ at the interface and those in the STO and anatase bulk regions, we see that the change in the bonding configuration at the interface drives the downward shift of the valence band. We will further discuss the evolution of the local electronic structure induced by the change in the bonding configuration in Sec. III B using the experimental EELS O K edge spectra across the interface.

To check the accuracy of the valence band offset computed within the LDA, we calculate quasiparticle (QP) corrections to the LDA eigenvalues using the GW method for bulk STO and TiO_2. The results are summarized in Table I. The band offset within the GW formalism is calculated as

$$\Delta E_{v\text{-}GW} = \Delta E_{v\text{-LDA}} - (\delta_{\text{STO}} - \delta_{\text{TiO}_2}), \qquad (7)$$

where $\Delta E_{v\text{-LDA}}$ is the valence band offset computed within DFT-LDA and δ_{STO} and δ_{TiO2} are the QP corrections to the LDA valence band maxima of $SrTiO_3$ and TiO_2, respectively. The

TABLE I. GW quasiparticle (QP) corrections for $SrTiO_3$ and anatase TiO_2.

Material	CBM, δ^a (k point/eV)	VBM, δ^a (k point/eV)
$SrTiO_3$	$\Gamma/1.9$, R/2.1	$\Gamma/-0.1$, R/−0.06
TiO_2	$\Gamma/1.97$, X/1.93	$\Gamma/-0.15$, X/−0.02

[a]δ's for the conduction band minimum (CBM) and the valence band maximum (VBM) are defined by E^{LDA}-E^{QP} at the CBM and VBM, respectively.

conduction band offset can be corrected in a similar manner. Since for computing band offsets we are interested only in the valence band maxima and the conduction band minima, we report only the QP corrections at the R and Γ k points for $SrTiO_3$, and at the Γ and X points for anatase. Using the values of δ_{STO} and δ_{TiO2} at these k points from Table I in Eq. (7), we find a GW correction of only 0.04 eV to the valence band offset calculated within LDA. Hence, although there is a significant QP correction to the band gaps of the individual bulk compounds, the valence band offset within the DFT-LDA is reliable, as most of the correction comes from the conduction band for both the compounds.

B. EELS O K edge spectra across the interface

Experimentally, the evolution of the electronic structure across the interface can be monitored using EELS.[65] We perform a similar measurement with atomic resolution across the region indicated in Fig. 3. We focus on the O K edge spectra[66–68] rather than the Ti $L_{2,3}$ edge spectra,[69–71] as the O K edge in STO and TiO_2 better reflects the change in the local bonding environment [see Fig. 9(a)].[65,72] Theoretically, to include the effect of core holes generated in experiment, we employ the so-called $Z+1$ approximation[73,74] in our calculations. We replace the O atom under investigation with fluorine and calculate the $2p$-projected DOS of the conduction band at that site.[72] In this way, one can create a positive charge in the core region and take into account the screening effect of the valence electrons. Using separate bulk calculations, we have, first, confirmed that increasing the in-plane cell size from 1×1 to $\sqrt{2}\times\sqrt{2}$ is sufficient to separate the core hole from its periodic images. We also find that the core-hole effect is small for the O K edge spectra, and we only use it to make a few important spectral features more pronounced. In Fig. 9(b), we plot the experimental EELS spectra along with the corresponding theoretical pDOS. Both are broadened using the Gaussian convolution method with a full width at half maximum value of 0.7 eV.

At the bottom of Fig. 9(b), we compare the O K edge spectrum taken from the STO bulk region to the $2p$ pDOS calculated at the O site in the STO bulk region of the supercell. In experiment, we observe three main features between 530 and 550 eV, which are well reproduced in theory. Analyzing the entire set of pDOS's, including contributions from the nearest neighbor Ti and Sr, we identify that the first, second, and third main peaks are derived from the interaction with Ti t_{2g}, Sr d, and Ti $4sp$ states, respectively. The Ti e_g peak is seen as a small peak in theory between the first t_{2g} and the second Sr d main peaks. However, as the e_g band is largely broadened in

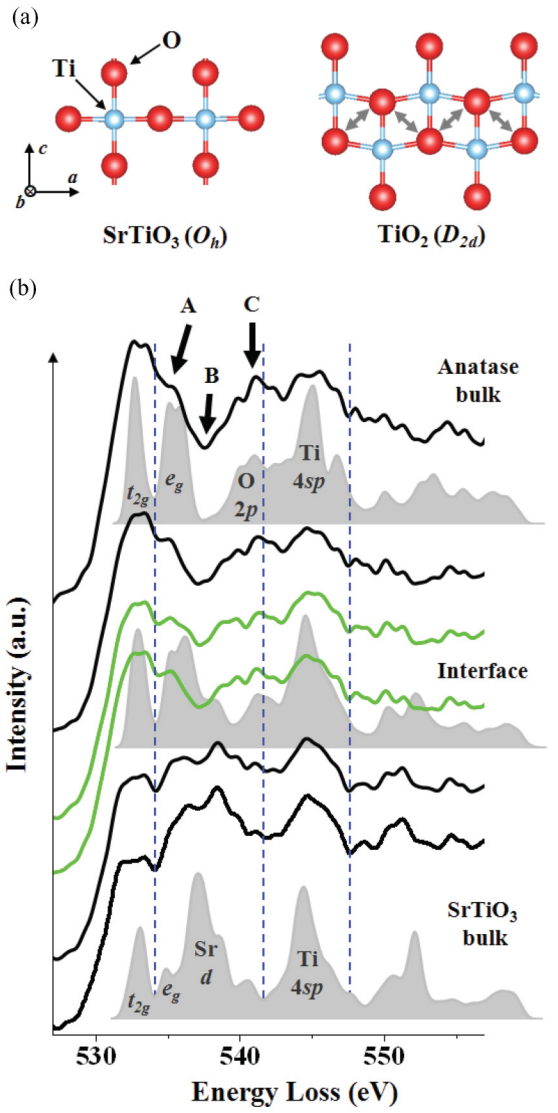

FIG. 9. (Color online) (a) Schematic pictures of a TiO_2 plane in bulk STO (left) and bulk anatase TiO_2 (right) (b) EELS O K edge spectra taken at the interface from the STO side (two bottom spectra) to the anatase TiO_2 side (two upper spectra) through the interface (two middle green spectra). The corresponding $2p$-projected DOS's are overlaid in grey.

STO with a bandwidth of about 5 eV, the e_g peak is not seen experimentally due to the presence of the adjacent large Sr d peak.

Looking at the spectrum taken from the anatase bulk region [see Fig. 9(b)], we observe quite different spectral features. First, the e_g and t_{2g} peaks become sharp and pronounced at position A compared to that of STO. Second, the Sr d peak is absent at position B, as there is no Sr on the TiO_2 side of the interface. Third, and most importantly, there is the appearance of a large spectral weight between 538 and 543 eV (position C), which is not found on the STO side. This peak turns out to be derived from the interaction with the nearest-neighbor O along the c axis. In Fig. 9(a) we show a schematic of the TiO_2 plane in STO and anatase. Although the basic building block in both materials is a TiO_6 octahedron, the connecting geometry differs: The octahedra share corners in STO while they share

four adjacent edges in anatase. In contrast to the straight Ti-O chain along the a or b axes in STO, it exhibits a zigzag pattern in anatase as shown in Fig. 9(a). In other words, for a given octahedron in anatase, two O atoms in the ab plane are shifted upward along the c direction and the other two are shifted down with respect to the central Ti atom. This crystallographic feature leads to appreciable π-type overlap between O $2p$ orbitals along the c direction as shown in Fig. 9(a). Finally, we remark that this spectral peak originally emerges at the interface, as shown in the middle of Fig. 9(b). By comparing with the $2p$ pDOS at the $O_{3\text{-fold}}$ site of the interfacial layer [site A in Fig. 5(a)], we infer that this peak at the interface reflects the chemical bond formation between anatase and STO.

C. Oxygen vacancy and fluorine impurity at the $TiO_2/SrTiO_3$ interface

DFT calculations reported in Ref. 31 suggested a valence band offset of 0.5 eV, consistent with our results but in apparent variance with the measurement. To better understand this discrepancy, we consider two types of interface defects, an oxygen vacancy and a substitutional fluorine impurity. For these calculations, we increase the in-plane cell size from 1×1 to $\sqrt{2} \times \sqrt{2}$ to allow for more structural degrees of freedom at the interface. We consider a six-ML-thick TiO_2 overlayer on STO(001).

In previous sections, we have established that interfacial O plays a crucial role in determining the dielectric response of the heterointerface. This brings forth a natural question: What would be the effect on the band alignment of an interfacial O vacancy?[75] Here we consider only a neutral vacancy. There are four types of interfacial O ions as shown in Fig. 5(a). We find that a vacancy at site B is the most stable configuration. The O vacancy formation energy at this site is calculated to be 3.8 eV while those of the A, C, and D sites are 1.6, 1.1, and 1.4 eV higher in energy, respectively. The formation energy of 3.8 eV is significantly lower than, for example, that of a neutral O vacancy in bulk STO, which is larger than 6.0 eV.[76] In Sec. III A, we have shown that O at site B is responsible for the screening of the interfacial dipole. Therefore, one can expect that the band offset would be significantly reduced by a vacancy at this site, as the charge transfer that tends to equilibrate the Fermi level of two oxides will not be fully screened. Using the average potential method, we calculate the band offset for the interface with a vacancy to be 0.04 eV, as shown in Fig. 10(a). The absence of the valence band offset in the presence of a vacancy is also seen in the pDOS of the heterostructure in Fig. 10(b).

In addition, we consider a substitutional F impurity at the STO surface, which could be present when the STO substrate is etched in buffered HF solution in order to have a 1×1 TiO_2-terminated surface.[31] It has been suggested in Ref. 31 that F substitutes for O at the STO surface and the mole fraction within the XPS probe depth (~45 Å) has been estimated to be about 5%. We consider all four interfacial O sites, A, B, C, and D, for the F substitution. We find that the most stable structure is obtained when F is substituted for twofold O at the B site. The relaxed structure for this configuration is shown in Fig. 11(a). F at the A, C, and D sites is higher in energy by 1.1, 0.7, and 0.8 eV, respectively. As mentioned earlier, twofold O

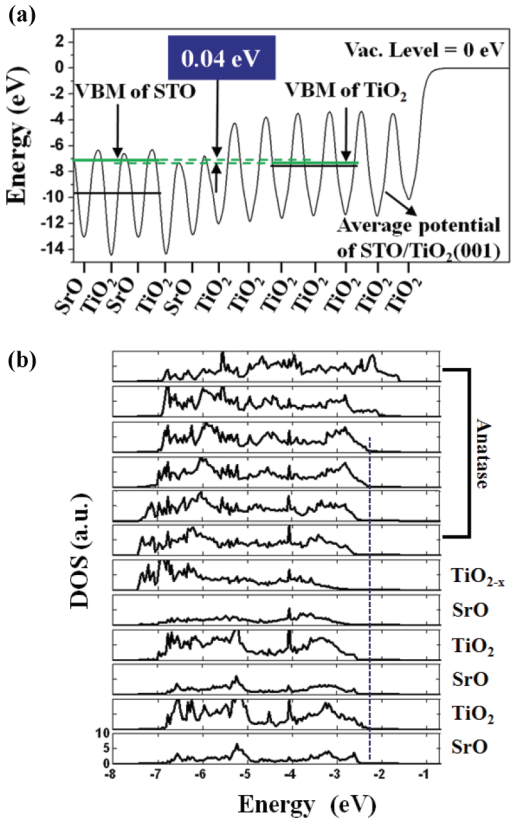

FIG. 10. (Color online) (a) Planar-averaged electrostatic potential of the heterostructure in the presence of an interfacial O vacancy. The straight black lines indicate the reference electrostatic energy positions with respect to the vacuum level. The green lines show the relative positions of VBM of $SrTiO_3$ and TiO_2 with respect to their reference energy positions. (b) Layer-by-layer valence band pDOS of the heterostructure in the presence of an interfacial O vacancy. The dotted straight line is placed at the VBM in the STO bulk region and is extended into the TiO_2 side for comparison.

at the B site is responsible for screening the interface dipole. Since F has lesser formal ionic charge of $-1e$ versus $-2e$ of O, one would expect that the effective charge of F at the interface is also reduced by about a factor of 2. Furthermore, as shown in Fig. 11(a), substituted F does not polarize, while the rest of twofold O on the STO surface polarize toward the STO side by 0.27 Å. We attribute this to a much shorter Ti-F bond length (1.75 Å in TiF_4 Ref. 77), as compared to the Ti-O bond length of 1.95 Å in STO. Therefore, we expect that the dielectric screening at the interface is significantly reduced by the F substitution. We plot the layer by layer pDOS in Fig. 11(b), showing a negligible valence band offset of less than 0.1 eV between STO and TiO_2 in the presence of F at the interface. The average potential method gives a comparable offset of 0.3 eV, which is consistent with the pDOS offset.

Thus, we argue that interfacial impurities, such as an O vacancy or substitutional fluorine, may be responsible for the experimentally observed absence of a valence band offset at the anatase TiO_2/STO interface.[31] It is worth noting that other mechanisms such as cationic exchange may also contribute to the disappearance of the valence band offset. For example, Ciancio *et al.* have observed a Sr-deficient epitaxial

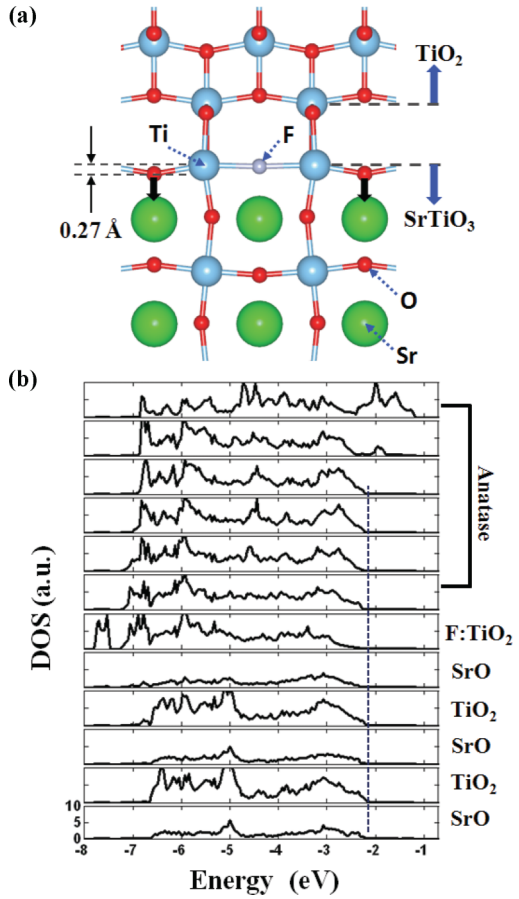

FIG. 11. (Color online) (a) Relaxed atomic structure of the $TiO_2/SrTiO_3(001)$ interface in the presence of an interfacial F impurity. (b) Layer-by-layer valence band pDOS of the heterostructure in the presence of the interfacial F impurity. The dotted line is placed at the VBM in the STO bulk region and extended across into the TiO_2 side for comparison.

interphase at the TiO_2/STO interface grown by pulsed laser deposition.[78,79] This interphase formation has been attributed to the long-range migration of Sr from the STO substrate to the anatase film.

IV. CONCLUSIONS

In summary, we studied the interfacial atomic structure and electronic structure of anatase TiO_2/STO(001) heterostructure grown on Si by molecular beam epitaxy using density function theory and scanning transmission electron microscopy. Theoretically, the interface is described at the local density approximation level. By analyzing the layer-by-layer pDOS and EELS O K edge spectra we show that the evolution of the valence band across the interface is driven by the change in bonding configuration. The main results are summarized as follows: (i) in the Schottky limit, the STO valence band top is higher in energy by 0.94 eV than that of TiO_2; (ii) charge transfer from STO to TiO_2 occurs mainly through the chemical bonds at the interface and equilibrates the Fermi level by forming a double layer. However, subsequent polarization of the $O_{2\text{-fold}}$ lattice largely screens the interfacial dipole, yielding a net valence band offset of 0.76 eV; (iii) the quasiparticle correction obtained with the GW method is large for the conduction band edge while the valence band edges of STO and TiO_2 are not altered. This supports the validity of the LDA result for the occupied valence band line-up; and (iv) comparing the EELS O K edge spectra and the $2p$-symmetry projected density of states across the interface, we show that the transition from O_h symmetry for TiO_6 with twofold coordinated O in STO to the tetragonal D_{2d} symmetry with threefold O in anatase drives the evolution of the valence band. One of the main features is the appearance of a π-type oxygen-oxygen interaction along the c direction. In addition, considering an interfacial O vacancy and F impurity, we show that the most stable vacancy or impurity site is the $O_{2\text{-fold}}$ site that is responsible for the screening of the dipole layer. As a result, the band offset is significantly reduced in the presence of O vacancy or F impurity at the interface suggesting that the perceived absence of a valence band offset[31] is not intrinsic.

ACKNOWLEDGMENTS

This work is supported by the National Science Foundation under Grant No. DMR-0548182, US Department of Energy (DOE) under Grant No. DE-SC0001878, Office of Naval Research under Grant No. N000 14-10-1-0489, and the Texas Advanced Computing Center.

*demkov@physics.utexas.edu

[1] B. O'Regan and M. Grätzel, Nature **353**, 737 (1991).
[2] A. Fujishima, X. Zhang, and D. A. Tryk, Surf. Sci. Rep. **63**, 515 (2008).
[3] X. Chen, S. Shen, L. Guo, and S. S. Mao, Chem. Rev. **110**, 6503 (2010).
[4] N. S. Lewis and D. G. Nocera, Proc. Natl. Acad. Sci. USA **103**, 15729 (2006).
[5] A. L. Linsebigler, G. Lu, and J. T. Yates, Chem. Rev. **95**, 735 (1995).
[6] H. G. Yang, C. H. Sun, S. Z. Qiao, J. Zou, G. Liu, S. C. Smith, H. M. Cheng, and G. Q. Lu, Nature **453**, 638 (2008).
[7] A. Selloni, Nat. Mater. **7**, 613 (2008).
[8] L. Forro, O. Chauvet, D. Emin, L. Zuppiroli, H. Berger, and F. Lévy, J. Appl. Phys. **75**, 633 (1994).
[9] H. Tang, K. Prasad, R. Sanjinès, and F. Lévy, J. Appl. Phys. **75**, 2042 (1994).
[10] M. Xu, Y. Gao, E. M. Moreno, M. Kunst, M. Muhler, Y. Wang, H. Idriss, and C. Wöll, Phys. Rev. Lett. **106**, 138302 (2011).
[11] F. E. Osterloh and B. A. Parkinson, MRS Bull. **36**, 17 (2011).
[12] R. Asahi, T. Morikawa, T. Ohwaki, K. Aoki, and Y. Taga, Science **293**, 269 (2001).
[13] Y. Gai, J. Li, S. S. Li, J. B. Xia, and S. H. Wei, Phys. Rev. Lett. **102**, 036402 (2009).
[14] W. Zhu, X. Qiu, V. Iancu, X.–Q. Chen, H. Pan, W. Wang, N. M. Dimitrijevic, T. Rajh, H. M. Meyer III, M. P. Paranthaman, G. M. Stocks, H. H. Weitering, B. Gu, G. Eres, and Z. Zhang, Phys. Rev. Lett. **103**, 226401 (2009).

[15]X. Chen, L. Liu, P. Y. Yu, and S. S. Mao, Science **331**, 746 (2011).
[16]T. Ohno, K. Sarukawa, K. Tokieda, and M. Matsumura, J. Catal. **203**, 82 (2001).
[17]D. C. Hurum, A. G. Agrios, and K. A. Gray, J. Phys. Chem. B **107**, 4545 (2003).
[18]N. Siedl, M. J. Elser, J. Bernardi, and O. Diwald, J. Phys. Chem. C **113**, 15792 (2009).
[19]D. L. Liao, C. A. Badour, and B. Q. Liao, J. Photochem. Photobiol. A **194**, 11 (2008).
[20]N. Nilius, T. Risse, S. Schauermann, S. Shaikhutdinov, M. Sterrer, and H.–J. Freund, Top. Catal. **54**, 4 (2011).
[21]S. A. Chambers, C. M. Wang, S. Thevuthasan, T. Droubay, D. E. McCready, A. S. Lea, V. Shutthanandan, and C. F. Wndisch Jr, Thin Solid Films **418**,197 (2002).
[22]Z. Wang, W. Zeng, L. Gu, M. Saito, S. Tsukimoto, and Y. Ikuhara, J. Appl. Phys. **108**, 113701 (2010).
[23]N. V. Burbure, P. A. Salvador, and G. S. Rohrer, Chem. Mater. **22**, 5823 (2010).
[24]D. Kazazis, S. Guha, N. A. Bojarczuk, A. Zaslavsky, and H.-C. Kim, Appl. Phys. Lett. **95**, 064103 (2009).
[25]R. Shao, C. Wang, D. E. McCready, T. C. Droubay, and S. A. Chambers, Surf. Sci. **601**, 1582 (2007).
[26]H. Ohta, S. Kim, Y. Mune, T. Mizoguchi, K. Nomura, S. Ohta, T. Nomura, Y. Nakanishi, Y. Ikuhara, M. Hirano, H. Hosono, and K. Koumoto, Nat. Mater. **6**, 129 (2007).
[27]Y. Matsumoto, M. Murakami, T. Shono, T. Hasegawa, T. Fukumura, M. Kawasaki, P. Ahmet, T. Chikyow, S. Koshihara, and H. Koinuma, Science **291**, 854 (2001).
[28]M. Katayama, S. Ikesaka, J. Kuwano, H. Koinuma, and Y. Matsumoto, Appl. Phys. Lett. **92**, 132107 (2008).
[29]T. C. Kaspar, T. Droubay, V. Shutthanandan, S. M. Heald, C. M. Wang, D. E. McCready, S. Thevuthasan, J. D. Bryan, D. R. Gamelin, A. J. Kellock, M. F. Toney, X. Hong, C. H. Ahn, and S. A. Chambers, Phys. Rev. B. **73**, 155327 (2006).
[30]Y. Yamada, K. Ueno, T. Fukumura, H. T. Yuan, H. Shimotani, Y. Iwasa, L. Gu, S. Tsukimoto, Y. Ikuhara, and M. Kawasaki, Science **332**, 1065 (2011).
[31]S. A. Chambers, T. Ohsawa, C. M. Wang, I. Lyubinetsky, and J. E. Jaffe, Surf. Sci. **603**, 771 (2009).
[32]M. Choi, A. Posadas, R. Dargis, C. Shih, and A. A. Demkov, J. Appl. Phys. **111**, 064112 (2012).
[33]G. Kresse and J. Furthmüller, Phys. Rev. B **54**, 11169 (1996).
[34]J. P. Perdew and A. Zunger, Phys. Rev. B **23**, 5048 (1981).
[35]P. E. Blöchl, Phys. Rev. B **50**, 17953 (1994).
[36]R. Loetzsch, A. Lübcke, I. Uschmann, E. Förster, V. Große, M. Thuerk, T. Koettig, F. Schmidl, and P. Seidel, Appl. Phys. Lett. **96**, 071901 (2010).
[37]D. R. Hummer, P. J. Heaney, and J. E. Post, Powder Diffr. **22**, 352 (2007).
[38]M. Shishkin and G. Kresse, Phys. Rev. B **74**, 035101 (2006).
[39]L. Hedin, Phys. Rev **139**, A796 (1965).
[40]M. S. Hybertsen and S. G. Louie, Phys. Rev. B **32**, 7005 (1985).
[41]W. Wei, X. Hu, Y. Liang, D. Jordan, B. Craigo, R. Droopad, Z. Yu, A. A. Demkov, J. Edward Jr., and W. Ooms, J. Vac. Sci. Technol. B **20**, 1402 (2002).
[42]R. A. McKee, F. J. Walker, and M. F. Chisholm, Phys. Rev. Lett. **81**, 3014 (1998).
[43]A. A. Demkov, L. R. C. Fonseca, E. Verret, J. Tomfohr, and O. F. Sankey, Phys. Rev. B **71**, 195306 (2005).
[44]O. Sharia, A. A. Demkov, G. Bersuker, and B. H. Lee, Phys. Rev. B **75**, 035306 (2007).
[45]X. Luo, G. Bersuker, and A. A. Demkov, Phys. Rev. B **84**, 195309 (2011).
[46]J. Junquera, M. Zimmer, P. Ordejón, and P. Ghosez, Phys. Rev. B **67**, 155327 (2003).
[47]K. Kita and A. Toriumi, Appl. Phys. Lett. **94**, 132902 (2009).
[48]A. Ohtomo and H. Y. Hwang, Nature **427**, 423 (2004).
[49]J. K. Lee and A. A. Demkov, Phys. Rev. B **78**, 193104 (2008).
[50]J. K. Lee, N. Sai, and A. A. Demkov, Phys. Rev. B **82**, 235305 (2010).
[51]M. Nakamura, A. Sawa, J. Fujioka, M. Kawasaki, and Y. Tokura, Phys. Rev. B **82**, 201101(R) (2010).
[52]R. A. McKee, F. J. Walker, M. B. Nardelli, W. A. Shelton, and G. M. Stocks, Science **300**, 1726 (2003).
[53]Y. Hikita, M. Nishikawa, T. Yajima, and H. Y. Hwang, Phys. Rev. B **79**, 073101 (2009).
[54]J. D. Burton and E. Y. Tsymbal, Phys. Rev. B **82**, 161407 (2010).
[55]L. Kleinman, Phys. Rev. B **24**, 7412 (1981).
[56]D. M. Bylander and L. Kleinman, Phys. Rev. B **36**, 3229 (1987).
[57]C. G. Van de Walle, Phys. Rev. B **39**, 1871 (1989).
[58]R. T. Tung, Phys. Rev. Lett. **84**, 6078 (2000).
[59]J. Tersoff, Phys. Rev. B **32**, 6968 (1985).
[60]R. M. Martin and K. Kunc, Phys. Rev. B **24**, 2081 (1981).
[61]Ph. Ghosez, J.–P. Michenaud, and X. Gonze, Phys. Rev. B **58**, 6224 (1998).
[62]M. Mikami, S. Nakamura, O. Kitao, and H. Arakawa, Phys. Rev. B **66**, 155213 (2002).
[63]R. J. Gonzalez, R. Zallen, and H. Berger, Phys. Rev. B **55**, 7014 (1997).
[64]C. J. Fennie and K. M. Rabe, Phys. Rev. B **68**, 184111 (2003).
[65]D. A. Muller, Nat. Mater. **8**, 263 (2009).
[66]F. M. F. de Groot, J. Faber, J. J. M. Michiels, M. T. Czyżyk, M. Abbate, and J. C. Fuggle, Phys. Rev. B **48**, 2074 (1993).
[67]K. van Benthem, C. Elsässer, and M. Rühle, Ultramicroscopy **96**, 509 (2003).
[68]D. A. Muller, T. Sorsch, S. Moccio, F. H. Baumann, K. Evans-Lutterodt, and G. Timp, Nature **399**, 758 (1999).
[69]R. Laskowski and P. Blaha, Phys. Rev. B **82**, 205104 (2010).
[70]K. Ogasawara, T. Iwata, Y. Koyama, T. Ishii, I. Tanaka, and H. Adachi, Phys. Rev. B **64**, 115413 (2001).
[71]P. Krüger, Phys. Rev. B **81**, 125121 (2010).
[72]D. A. Muller, D. J. Singh, and J. Silcox, Phys. Rev. B **57**, 8181 (1998).
[73]C. Elsässer and S. Köstlmeier, Ultramicroscopy **86**, 325 (2001).
[74]G. Duscher, R. Buczko, S. J. Pennycook, and S. T. Pantelides, Ultramicroscopy **86**, 355 (2001).
[75]X. Weng, P. Fisher, M. Skowronski, P. A. Salvador, and O. Maksimov, J. Cryst. Growth. **310**, 545 (2008).
[76]C. Mitra, C. Lin, J. Robertson, and A. A. Demkov (submitted for publication).
[77]K. D. Dobbs and W. J. Hehre, J. Comp. Chem. **8**, 880 (1987).
[78]R. Ciancio, E. Carlino, C. Aruta, D. Maccariello, F. M. Granozio, and U. S. di Uccio, Nanoscale **4**, 91 (2012).
[79]M. Radović, M. Salluzzo, Z. Ristić, R. di Capua, N. Lampis, R. Vaglio, and F. M. Granozio, J. Chem. Phys. **135**, 034705 (2011).